Polarized neutron studies of CeNiSn

1997 J. Phys.: Condens. Matter 9 9321

(http://iopscience.iop.org/0953-8984/9/43/016)

J. Phys.: Condens. Matter **9** (1997) 9321–9332. Printed in the UK PII: S0953-8984(97)84003-9

Polarized neutron studies of CeNiSn

A Hiess†‡+, I Zobkalo†§, M Bonnet†, J Schweizer†, E Lelièvre-Berna‖, F Tasset‖, Y Isikawa¶ and G H Lander‡

† Département de Recherche Fondamentale sur la Matière Condensée, CEA-Grenoble, F-38054 Grenoble Cédex 9, France

‡ European Commission, JRC, Institute for Transuranium Elements, Postfach 2340, D-76125 Karlsruhe, Germany

§ Petersburg Nuclear Physics Institute, 188350 Gatchina, Russia

‖ Institut Laue–Langevin, BP 156, F-38042 Grenoble Cédex 9, France

¶ Department of Physics, Toyama University, Toyama 930, Japan

Received 7 May 1997

Abstract. To achieve a deeper understanding of the hybridization process in the so-called 'low-charge-carrier Kondo system', the magnetization density within the unit cell, induced by an external magnetic field, has been investigated by means of polarized neutron diffraction for single crystals of CeNiSn. As expected, most of the induced moment is associated with the Ce 4f electrons at the Ce site, but a significant magnetization density has also been observed at the Ni site. This observation is evidence that the Ni 3d band is not filled, and confirms recent band-structure calculations that suggest the Ce 4f–Ni 3d hybridization to be fundamental to the production of a 'gap' at the Fermi level in CeNiSn. We suggest that this hybridization process is the cause of the anisotropy of the physical properties of this material.

1. Introduction

CeNiSn is considered as a so-called 'Kondo insulator' or more precisely a 'low-charge-carrier-density Kondo system', its properties resulting from the hybridization of the Ce 4f electrons with the conduction electrons. Many of its physical properties are anisotropic (for more details see the review article by Takabatake and Fujii [1]). Recent transport measurements of the purest materials point to a ('pseudo-gapped') metallic ground state with a very low charge-carrier density [2]. Inelastic neutron studies [3, 4] have established that there are two types of spatial correlation occurring on energy scales of 2 and 4 meV. These are thought to reflect the nature of the Kondo coherent state in CeNiSn. More recently, Hammond *et al* [5] have performed self-consistent first-principles band-structure calculations for the isostructural compounds CeTSn (T = Ni, Pd, and Pt) and claim that there is a significant difference between CeNiSn, on the one hand, and CePdSn and CePtSn on the other. They obtain a 'gap', albeit larger than that found experimentally, only in the case of the Ni compound, and show that the hybridization with the Ni 3d electrons accounts for many of the special features of CeNiSn. In addition, from photoemission studies of the same compounds [6] it has been concluded that (a) the Ce–Sn hybridization is strong in all three compounds and (b) only in CeNiSn has Ce–T hybridization been observed.

Our studies set out to answer a number of questions. The first one—possibly only indirectly related to the physics of CeNiSn—is that of whether the structure of this

+ Present address: ILL, BP 156, F-38042 Grenoble Cédex 9, France.

0953-8984/97/439321+12$19.50

compound is indeed the centrosymmetric ϵ-TiNiSi ($Pnma$, No 62) structure [7] or its non-centrosymmetric variation ($Pn2_1a$, No 33) as recently suggested [8]. The second aspect was to determine the magnetization density in the unit cell of CeNiSn when a magnetic field is applied. This gives a measure of the ground state, and, in particular, should be able to show whether there is any unpaired-electron density associated with the Ni 3d states. A third aim was to examine the form factor of the magnetization density around the Ce site to determine whether there is any quenching of the orbital moment, again a process that often accompanies hybridization. Finally, together with the magnetization experiments, the results of the neutron experiments can be used to deduce the conduction electron polarization.

2. Experimental details

2.1. Sample preparation and magnetization measurements

A large single crystal of size about 1 cm^3 with the growth direction parallel to the *b*-axis was grown by the Czochralski method [9] starting from high-purity elements. Similar samples were used earlier for inelastic neutron experiments [4]. Three different pieces of this crystal were cut: first (sample A) a bar elongated along the *a*-axis ($7 \times 2 \times 3.5$ mm^3), second (sample B) a bar elongated along the *b*-axis ($3 \times 8 \times 3$ mm^3), and third (sample C) a small triangular sample of $V = 4$ mm^3. The samples were characterized by magnetization measurements using a QD SQUID magnetometer at CEA-Grenoble. Some high-field data are shown in figure 1. Our results are consistent with the literature [1].

Table 1. Experimental details of the investigation of the integrated intensities used for the structural refinement.

Instrument	λ (Å)	Sample	T (K)	Different reflections
DN4	1.176	A	300	1623
DN4	1.176	A	6	1258
DN4	1.176	C	300	1921
DN4	1.176	C	6	1292
D3	0.843	B	2	56
D3	0.711	B	2	41
D3	0.514	B	2	41

2.2. Crystallographic studies

Neutron diffraction experiments were performed on samples A and C using the four-circle diffractometer DN4 ($\lambda = 1.176$ Å) of the Siloé reactor (CEA-Grenoble) to examine the crystal structure, the sample quality and the influence of extinction. Additional integrated intensities were measured on the (polarized neutron) lifting-arm diffractometer D3 of ILL at various wavelengths. The experimental details are given in table 1. The lattice parameters change from $a = 7.542(1)$ Å, $b = 4.601(1)$ Å, and $c = 7.617(1)$ Å at room temperature to $a = 7.500(1)$ Å, $b = 4.580(1)$ Å, and $c = 7.580(1)$ Å at 6 K. We used a standard least-squares refinement procedure (MXD and MK4) for the determination of the crystallographic parameters. The neutron coherent scattering lengths used were $b_{Ce} = 4.84$ fm, $b_{Ni} = 10.30$ fm, and $b_{Sn} = 6.23$ fm. The function minimized during the least-squares refinement was $\sum w|F_{obs} - F_{calc}|^2$, with $w = 1/\sigma^2$. Absorption and

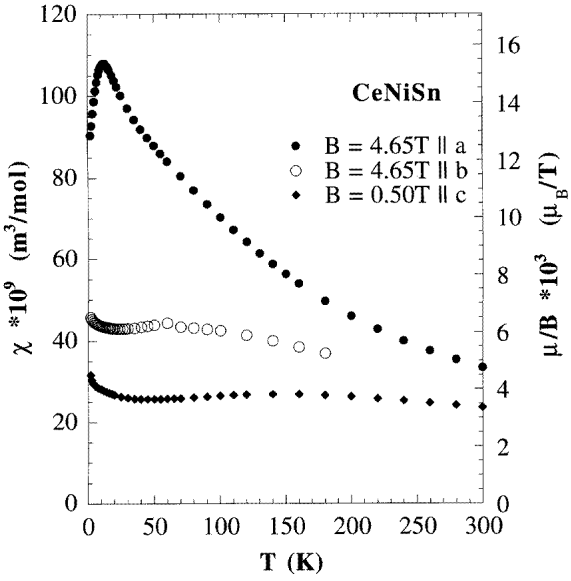

Figure 1. M/B (induced moment per tesla) for CeNiSn as a function of temperature. The external magnetic field for $\boldsymbol{B}\|\boldsymbol{a}$ and $\boldsymbol{B}\|\boldsymbol{b}$ corresponds to the (lower) field used in the polarized neutron experiments.

extinction corrections [10] as well as anisotropic temperature factors were applied. The final goodness of the best fit of the structure factors for the small single crystal (sample C) was $R_w = (\sum w||F_{obs}| - |F_{calc}||)/(\sum w|F_{obs}|) \approx 2\%$. The structure factor refinements using the two proposed space groups ($Pnma$ and $Pn2_1a$) are very similar, and the results are compared to those of Higashi *et al* [8] in table 2.

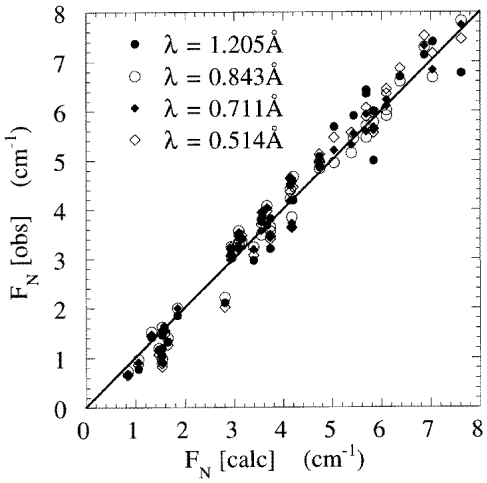

Figure 2. Observed scattering amplitudes plotted versus the calculated structure factors from measurements at different wavelengths. No deviation from the expected straight line has been observed, showing that extinction effects are reasonably small.

Table 2. The least-squares refinement of the structure factors from the four-circle data, taken on the DN4 diffractometer of Siloé at different temperatures and for two parts of one crystal. The crystal structure of CeNiSn was refined by using both proposed space groups. The results of a recent x-ray work [7] are reproduced for comparison. The significance is about one unit in the last digit shown. Abbreviations used: L: literature value, S: fixed by symmetry, F: fixed in refinement, —: not reported.

Sample	A		A		C		C		Reference [7]	
T (K)	300		6		300		6		300	
a (Å)	7.542 L		7.500		7.542 L		7.500		7.542	
b (Å)	4.601 L		4.578		4.601 L		4.580		4.601	
c (Å)	7.617 L		7.580		7.617 L		7.579		7.617	
Group	No 62	No 33	No 62	No 33	No 62	No 33	No 62	No 33	No 62	No 33
R (%)	3.9	3.8	3.1	2.7	2.6	2.6	2.6	2.5	4.6	4.4
R_w (%)	3.6	3.5	3.4	3.1	1.5	1.5	1.4	1.4	3.8	3.6
χ^2	31.8	30.7	36.3	31.2	2.9	2.8	2.5	2.4	—	—
x_{Ce}	0.4819		0.4813		0.4818		0.4814		0.4817	
y_{Ce}	0.25 S	0.25 F	0.25 S	0.25 F	0.25 S	0.25 F	0.25 S	0.25 F	0.25 S	0.25 F
z_{Ce}	0.1964		0.1949		0.1969		0.1958		0.1970	
x_{Ni}	−0.3107		−0.3102		−0.3108		−0.3103		−0.3108	
y_{Ni}	0.25 S	0.247	0.25 S	0.264	0.25 S	0.256	0.25 S	0.260	0.25	0.252
z_{Ni}	−0.4182		−0.4177		−0.4180		−0.4174		−0.4179	
x_{Sn}	−0.1857		−0.1844		−0.1856		−0.1842		−0.1857	
y_{Sn}	0.25 S	0.241	0.25 S	0.263	0.25 S	0.254	0.25 S	0.257	0.25	0.243
z_{Sn}	−0.0907		−0.0903		−0.0908		−0.0906		−0.0908	
g (rad^{-1})	220	190	470	360	390	370	450	410	—	—

Because relatively large samples have to be used for the polarized neutron work, extinction effects have been carefully checked. The refinement of the four-circle data shows that the influence of extinction is reasonably small, affecting the strongest reflections by less than 15%, and a mosaicity of $\eta = (2\sqrt{\pi}g)^{-1} \approx 3'$ has been deduced. The weak influence of extinction has been confirmed by measurements of integrated intensities at different wavelengths. Extinction is strongly dependent on the wavelength ($I/I_{calc} \propto \lambda^3/\sin 2\Theta$) but even for the longest wavelength no significant deviation from the calculated intensities has been observed as can be seen in figure 2.

2.3. Polarized neutron studies

Flipping ratios $R = I^+/I^-$ were measured in external magnetic fields of $B = 4.6$ T and $B = 8$ T, applied parallel to both the a- and b-axis, using the polarized neutron diffractometers DN2 of the Siloé reactor and D3 of ILL. The experimental details are summarized in table 3. About 50 flipping ratios were measured in each field orientation at various temperatures ($T = 2$ K, 4 K, 12 K, 50 K) and some even at four different wavelengths.

In the case of a centrosymmetric crystal structure, and if the nuclear structure factors $F_N(\boldsymbol{q})$ are known, the magnetic structure factors $F_M(\boldsymbol{q})$ can be determined from the flipping ratios. The magnetic structure factors are the Fourier components of the magnetization density $M(\boldsymbol{r})$ [11], and therefore the magnetization density can be reconstructed by using Fourier transformation or a so-called 'three-dimensional maximum-entropy treatment'. The latter is a model-free algorithm, which calculates the most probable density map of the

Table 3. Experimental details of the flipping ratio measurements with polarized neutrons to determine the magnetic structure factors.

Instrument	λ (Å)	Sample	T (K)	B	Different reflections
DN2	1.205	A	2	8.0 T $\|\|a$	23
DN2	1.205	A	4	8.0 T $\|\|a$	31
DN2	1.205	A	12	8.0 T $\|\|a$	31
DN2	1.205	A	50	8.0 T $\|\|a$	31
DN2	1.205	A	2	4.6 T $\|\|a$	8
DN2	1.205	A	12	4.6 T $\|\|a$	8
DN2	1.205	A	50	4.6 T $\|\|a$	8
D3	0.843	A	12	4.6 T $\|\|a$	48
D3	0.711	A	12	4.6 T $\|\|a$	8
D3	0.514	A	12	4.6 T $\|\|a$	6
D3	0.843	B	2	4.6 T $\|\|b$	52
D3	0.711	B	2	4.6 T $\|\|b$	10
D3	0.514	B	2	4.6 T $\|\|b$	10
D3	0.843	B	12	4.6 T $\|\|b$	35
D3	0.843	B	50	4.6 T $\|\|b$	35

magnetization compatible with the experimental results [12]. Loosely speaking, this procedure assumes 'reasonable' values for all magnetic structure factors not measured and considers also the error of the measured ones, whereas simple Fourier transformation assumes all unmeasured magnetic structure factors to be zero and treats the measured ones as 'exact'. The atomic positions are not used in the reconstruction process. The preferred solution for the maximum entropy is a flat, uniform magnetization density in the unit cell, because any deviation from 'uniformity' costs entropy. It is possible to include a prior model and to define the maximum-entropy function so that it 'prefers' the magnetization-density map of the model, if it is consistent with the measurements.

Assumptions about the phase factors are needed to extract the magnetic structure factors in the case of a non-centrosymmetric structure, because the phase cannot be determined by this kind of diffraction experiment. Nevertheless, the maximum-entropy method allows one to reconstruct the most probable magnetization-density map directly from the flipping ratios by handling the phases as undetermined parameters [13].

The data were treated in three different ways. First, the magnetization density was reconstructed directly from the flipping ratios, assuming the non-centrosymmetric space group $Pn2_1a$, and the parameters from the x-ray refinement of Higashi *et al* [8] were used to calculate the nuclear structure factors. Second, the reconstruction was performed by using the same reconstruction algorithm for the flipping ratios but assuming the centrosymmetric space group $Pnma$. Finally we extracted the magnetic structure factors from the flipping ratios, assuming CeNiSn to be centrosymmetric, and reconstructed the magnetization density with the conventional maximum-entropy procedure.

3. Discussion

3.1. Crystallography

Our crystal refinements are unable to establish any significant difference between the centrosymmetric ($Pnma$) and the non-centrosymmetric space group ($Pn2_1a$). The crucial

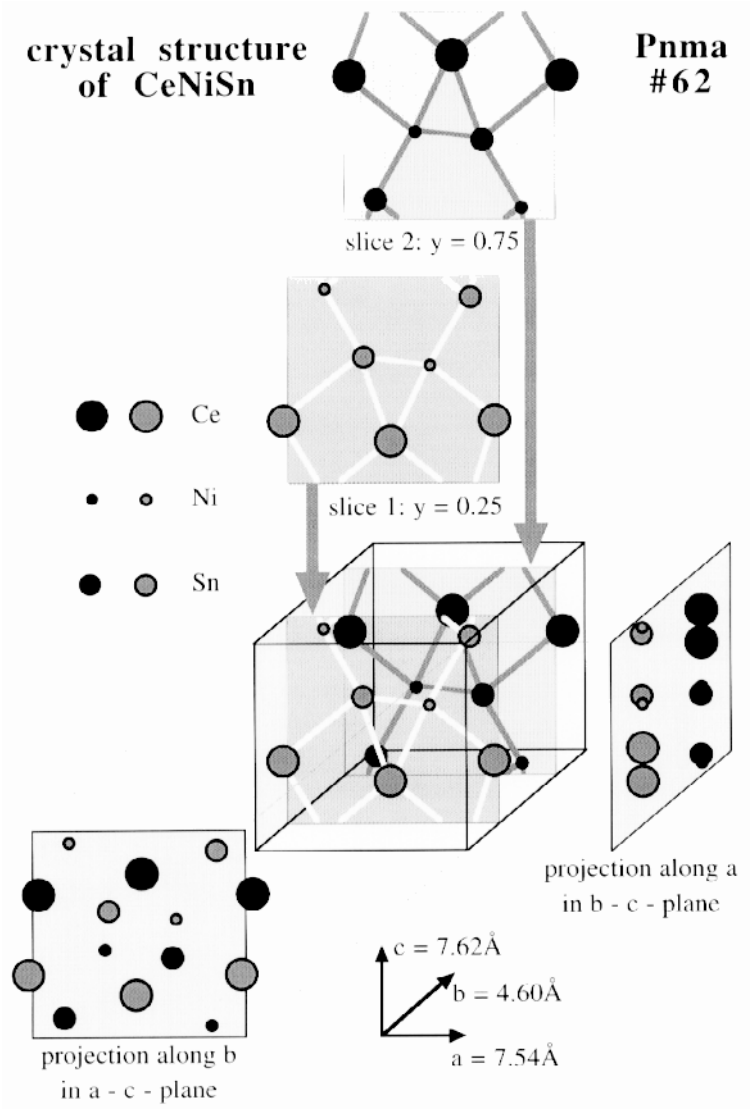

Figure 3. The crystal structure of CeNiSn. The projections onto the a–c and b–c planes represent the projections made in the polarized neutron data treatment.

parameters are y_{Ce}, y_{Ni} and y_{Sn}, which are fixed by symmetry at $y = 0.25$ in $Pnma$. When fixing the parameter $y_{Ce} = 0.25$—which defines the origin—in the space group $Pn2_1a$ the other y-values found by Higashi *et al* [8] are $y_{Ni} = 0.2521$ and $y_{Sn} = 0.2433$. Our refined values for the y_{Ni} and y_{Sn} vary from about 0.24 to 0.27 depending on the data set and the refinement procedure. It appears to us that the crystal structure of CeNiSn is sufficiently well described by the centrosymmetric space group $Pnma$, especially because the final goodness of the fit is not significantly changed by using two additional parameters in the non-centrosymmetric space group. We stress that which space group is used does not change the results for the magnetism. The other atomic positions extracted from the different data sets are in excellent agreement with the ones in the literature. As we have already pointed

out earlier, the extinction effects are reasonably small, affecting the strongest reflections by less than 15%. As expected, all of the temperature factors (not given in the table 2) are smaller at low temperatures than at room temperature. The temperature factors are found to be almost isotropic at all temperatures; only the temperature factor ellipsoid of the Ni seems to be elongated along the *a*-axis at room temperature as well as at low temperatures. We used the refined crystallographic parameters and selected the centrosymmetric space group *Pnma* for the following analysis. The crystal structure of CeNiSn is shown in figure 3. The structure is made up of two rotated sheets each containing two Ce, Ni, and Sn atoms stacked along the *b*-axis. Three shortest Ce–Ce distances of about 3.8 Å exist, in addition to the two almost along the *a*-axis, in one sheet. But two out of four Ce–Ni distances are shorter than 3.5 Å, forming Ce–Ni zig-zag lines along the *a*-axis.

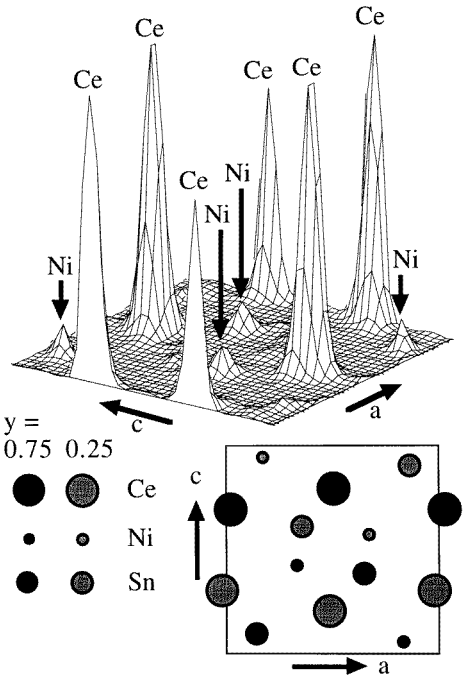

Figure 4. A spin-density map of CeNiSn at $T = 12$ K reconstructed by means of three-dimensional maximum-entropy treatment with magnetic field $B = 4.6$ T $\|\boldsymbol{b}$, projected onto the *a*–*c* plane as a 3D presentation. The atomic positions are marked.

3.2. Magnetism

The magnetization-density maps obtained from the reconstruction by the three different maximum-entropy procedures described above are very similar. As examples we show the reconstruction by means of the conventional maximum-entropy method in figure 4 in a 3D representation, and in figure 5 as projections onto the horizontal plane of the experiment. A small induced moment has been observed at the nickel position in addition to the magnetization density on the cerium in external fields of $B = 4.6$ T applied parallel to the *a*- or *b*-axis. This magnetization density seems to be slightly displaced along the *c*-axis towards the Ce atoms in a magnetic field of $B = 8.0$ T. Again, these results are

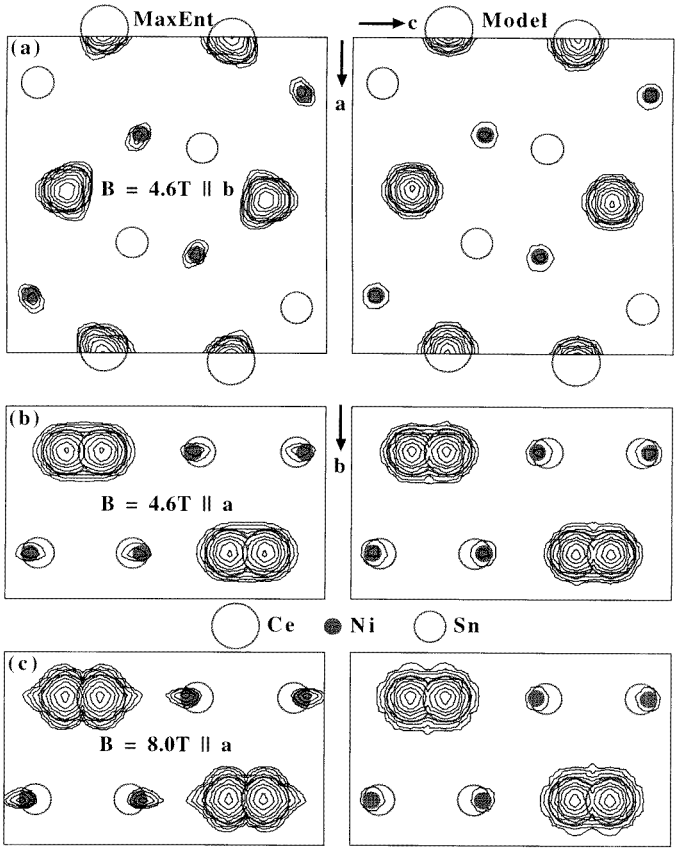

Figure 5. Left-hand panels: the spin-density map of CeNiSn at $T = 12$ K reconstructed by means of a three-dimensional maximum-entropy treatment (a) with magnetic field $B = 4.6$ T $\|\boldsymbol{b}$, projected onto the a–c plane, (b) with magnetic field $B = 4.6$ T $\|\boldsymbol{a}$, projected onto the b–c plane, (c) with magnetic field $B = 8.0$ T $\|\boldsymbol{a}$, projected onto the b–c plane. In addition to the induced magnetic moment on the cerium, a small magnetic moment on the nickel has been observed. The projection corresponds to the projections shown in figure 3. Right-hand panels: the calculated magnetization density calculated with the parameters from the least-squares refinement as described in the text. The scale is logarithmic and the lowest contour corresponds to 2% of the total moment.

independent of the space group and the algorithm used for the reconstruction process.

Further quantitative results were obtained by a least-squares refinement of the magnetic structure factors extracted. We assume a variable (spin) moment on the nickel (Ni^{2+}) and describe the cerium by a Ce^{3+} form factor in the dipole approximation. The magnetic structure factor can be written as

$$F_{\mathrm{M}} = m_{\mathrm{Ni}}\langle j_0\rangle_{\mathrm{Ni}} \sum_{\mathrm{Ni}} \exp(-2\pi \mathrm{i}\boldsymbol{q}\cdot\boldsymbol{r}) + m_{\mathrm{Ce}}(\langle j_0\rangle_{\mathrm{Ce}} + c_2\langle j_2\rangle_{\mathrm{Ce}}) \sum_{\mathrm{Ce}} \exp(-2\pi \mathrm{i}\boldsymbol{q}\cdot\boldsymbol{r}).$$

In table 4 we show the results of our refinement (model 2). The total induced magnetic moment is temperature and field dependent as expected from the bulk magnetization, but for all experiments about (6 ± 2)% of the total moment is associated with the nickel. The goodness of the fit decreases drastically on neglecting the moment on the nickel (model 1),

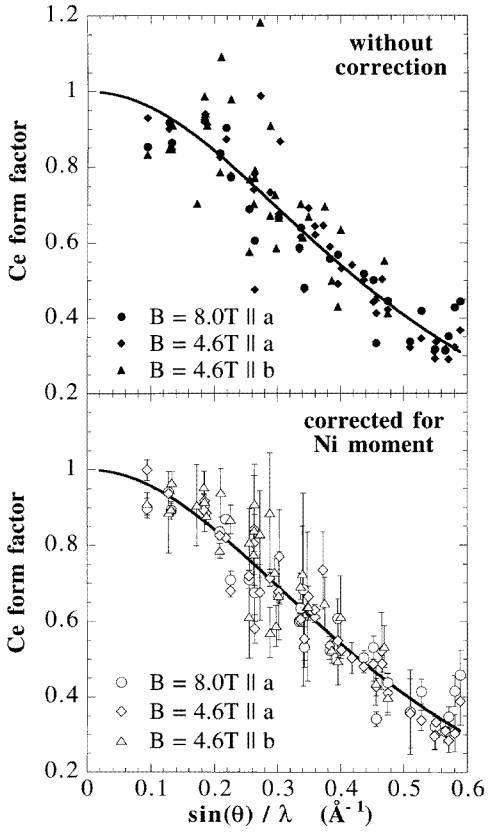

Figure 6. Top: the Ce form factor as deduced by neglecting the moment on the nickel site. Bottom: the Ce form factor as deduced by assuming a small moment on the nickel site as described in the text. The solid line is a fit to the free-ion Ce^{3+} form factor in the dipole approximation $f = \langle j_0 \rangle + c_2 \langle j_2 \rangle$.

but it is less sensitive to the c_2-value, which was fixed at $c_2 = 1.33$, the conventional free-ion value of Ce^{3+} in the dipole approximation, in the refinements shown in table 4. The cerium form factor as deduced by neglecting the magnetization on the nickel is shown in the top part of figure 6, and that deduced after correcting for the nickel contribution is shown in the lower part. It is quite well described by the dipole approximation with $c_2 = 1.33(10)$, corresponding to $-\mu_L/\mu_S = c_2/(c_2 - 1) = 4$. The sum of the nickel and cerium moments is, within the precision of our experiment, equal to the total moment deduced from the bulk magnetization, and hence any delocalized (conduction electron) polarization is very small.

To complete the analysis, we calculated magnetization-density maps corresponding to our refinement (model 2), which are compared to the maximum-entropy maps in figure 5. For the lower field $B = 4.6$ T the two maps are consistent. The agreement is less convincing in high magnetic fields, because a displacement of the Ni moment has not been included in the model. To be sure that the displacement observed in high magnetic fields is not an artefact of the model-free maximum-entropy reconstruction, we used the calculated magnetization density as the prior model for the maximum-entropy algorithm. Nevertheless (and at a cost of entropy) the resulting maps confirm unambiguously a displacement of the magnetization around the nickel. A subsequent least-squares refinement similar to the

Table 4. Results of a least-squares refinement of the induced magnetic moments carried out by assuming moments on the cerium only (model 1), on the cerium and nickel sites (model 2) and by allowing a displacement of the nickel moment (model 3) as described in the text. The total moment was determined by bulk magnetization measurements, and $m_{CEP} = m_{bulk} - (m_{Ce} + m_{Ni})$.

Sample	B (T)	T (K)	Model	μ_{Ce} (μ_B)	μ_{Ni} (μ_B)	Δz_{Ni} (r.l.u.)	R_w (%)	μ_{tot} (μ_B)	μ_{CEP} (μ_B)
A	8.0	2	1	0.097(2)	—	—	8.4		
			2	0.099(1)	0.009(2)	—	6.4		
			3	0.099(1)	0.009(1)	0.01(1)	6.3	0.103	−0.004(3)
A	8.0	4	1	0.098(2)	—	—	10.4		
			2	0.100(2)	0.008(2)	—	8.0		
			3	0.100(2)	0.008(2)	0.03(1)	7.3	0.109	0.001(3)
A	8.0	12	1	0.114(2)	—	—	10.3		
			2	0.115(2)	0.006(2)	—	9.0		
			3	0.115(2)	0.009(2)	0.05(1)	7.8	0.123	−0.001(4)
A	8.0	50	1	0.094(2)	—	—	10.3		
			2	0.095(2)	0.004(2)	—	9.5		
			3	0.095(2)	0.005(2)	0.03(1)	9.0	0.100	0.001(4)
A	4.6	12	1	0.0668(9)	—	—	8.6		
			2	0.0668(6)	0.0051(7)	—	6.0	0.0716	0.000(1)
B	4.6	2	1	0.0241(4)	—	—	11.5		
			2	0.0246(3)	0.0017(2)	—	8.4	0.0302	0.004(1)
B	4.6	12	1	0.0240(5)	—	—	12.0		
			2	0.0244(3)	0.0021(3)	—	7.9	0.0289	0.002(1)
B	4.6	50	1	0.0252(4)	—	—	9.6		
			2	0.0256(3)	0.0017(2)	—	6.0	0.0292	0.002(1)

one described above, but with an additional free parameter z_{Ni} to allow some displacement along the c-axis, led to slightly improved goodness of the fit only in the case of $B = 8$ T (model 3 in table 4).

3.3. The hybridization process

The principal result of our investigation of the magnetization density of CeNiSn is that there is a small ($(6 \pm 2)\%$) moment associated with the nickel site. This suggests that the Ni 3d band is not filled. Such a conclusion is in excellent agreement with the band-structure calculations of Hammond *et al* [5] who have predicted a 9% Ni 3d and 3% Sn 5p character of the electron band at the Fermi level. Moreover, they emphasize that this derives from hybridization, and they suggest that this is the cause of the anisotropic 'gap' in CeNiSn. We stress that our results are also consistent with the photoemission studies of Nohara *et al* [6] but because no significant polarization at the Sn site has been observed we conclude that the Ce–Ni hybridization is stronger than the Ce–Sn hybridization. Since we have not made similar studies on CePdSn and CePtSn we cannot at this stage say whether this effect is absent in these compounds. Within the precision of our measurements the effect is independent of temperature, i.e. it scales with the susceptibility. This shows that it is a ground-state property, and not related to the formation of the Kondo state at

low temperature. It is the latter, of course, that is probed by neutron inelastic scattering. However, in theories aimed at explaining the formation of the Kondo state, the occupation of the Ni 3d band, and the hybridization between the Ce 4f and Ni 3d electrons must be considered.

The form factor of the Ce magnetization density appears little modified from that of a free ion in the Ce^{3+} state. Again, the precision of the measurements may not be sufficient to show small subtle changes, but any large modification is excluded, so the induced moment remains dominated by a large orbital part. The conduction electron polarization, obtained by subtracting the sum of the moments on the Ce and Ni atoms from the total bulk magnetization, is negligible (the last column of table 4). Normally in the light-electron (i.e. with less than half-filled shells) systems one would expect $m_{\mathrm{CEP}} < 0$, because the conduction band will be polarized parallel to the spin of the localized electrons, and, at least for f electrons, the orbital moments dominate for the lighter elements. The final conduction electron polarization should therefore be antiparallel to the total magnetization. However, for most cerium compounds it has been found to be positive, and Pavarini *et al* [14] have discussed this aspect of the form factor and conclude that a positive conduction electron polarization in the case of cerium compounds is a consequence of hybridization. In this compound the conduction electron polarization is at least very small, and this may be a consequence of the special hybridization process involving the Ni 3d electrons, which leads finally to a very low charge-carrier density. It is tempting to assume the conduction electron polarization to be correlated with the quantity of charge carriers.

The last aspect is the observed displacement of the nickel magnetization in high magnetic fields towards its neighbouring Ce atom. A field-dependent and anisotropic Ce–Ni hybridization process with the main component perpendicular the *a*-axis might cause *a* to be the easy axis and could be the origin for the observed anisotropy of many physical properties in CeNiSn.

4. Conclusion

Our polarized neutron experiments show that the hybridized Ni 3d band of CeNiSn is not filled, and therefore a magnetization at the nickel site has been observed in an applied magnetic field. This result is consistent with band-structure calculations [5] claiming some remaining Ni 3d character for the closest conduction electron band. This small moment and the very small value of any conduction electron polarization has to be taken into account when describing the hybridization process of CeNiSn. The 4f–3d hybridization might result in the *a*-axis being the easy one, and this could be the origin for the observed anisotropy of many physical properties in CeNiSn.

Acknowledgments

We thank Jacques Flouquet and Andrei Mishchenko for a number of discussions. Support given to AH within the framework of the EC-funded training programme HCM is acknowledged.

References

[1] Takabatake T and Fujii H 1993 *Phys. Prop. Actinides Rare Earth Compounds (Japan. J. Appl. Phys. Series)* **8** 254

[2] Hiess A, Geibel C, Sparn G, Bredl C D, Steglich F, Takabatake T and Fujii H 1994 *Physica* B **199+200** 437

Nakamoto G, Takabatake T, Bando Y, Fujii H, Izawa K, Suzuki T, Fujita F, Minami A, Oguro I, Tai L T and Menovsky A A 1995 *Physica* B **206+207** 840
[3] Mason T E, Aeppli G, Ramirez A P, Clausen K N, Broholm C, Stücheli N, Bucher E and Palstra T T M 1992 *Phys. Rev. Lett.* **69** 490
[4] Sato T, Kadowaki H, Yoshizawa H, Ekino T, Takabatake T, Fujii H, Regnault L P and Isikawa Y 1995 *J. Phys.: Condens. Matter* **7** 8009
[5] Hammond T J, Gehring G A, Suvasini M B and Temmerman W M 1995 *Phys. Rev* B **51** 2994
[6] Nohara S, Namatame H, Fujimori A and Takabatake T 1993 *Phys. Rev*. B **47** 1754
[7] Skolozdra R V, Koreskaya O E and Gorelenko Y K 1984 *J. Inorg. Mater*. **20** 604
[8] Higashi I, Kobayashi K, Takabatake T and Kawaya M 1993 *J. Alloys Compounds* **193** 300
[9] Isikawa Y, Mori K, Ogisi Y, Oyaba K and Sato T 1991 *J. Phys. Soc. Japan* **60** 2514
[10] Becker P J and Coppens P 1974 *Acta Crystallogr*. A **30** 129
[11] Schweizer J and Tasset F 1980 *J. Physique* **10** 2799
[12] Papoular R J and Gillon B 1990 *Neutron Scattering Data Analysis (Inst. Phys. Conf. Ser. 107)* (Bristol: Institute of Physics Publishing)
[13] Schleger P, Puig-Molina A, Ressouche E, Rutty O and Schweizer J 1997 *Acta Crystallogr*. A **53** 426
[14] Pavarini E, Andreani L C and Amoretti G 1995 *Physica* B **206+207** 144